J. Fluid Mech. (2022), *vol*. 944, A55, doi:10.1017/jfm.2022.528

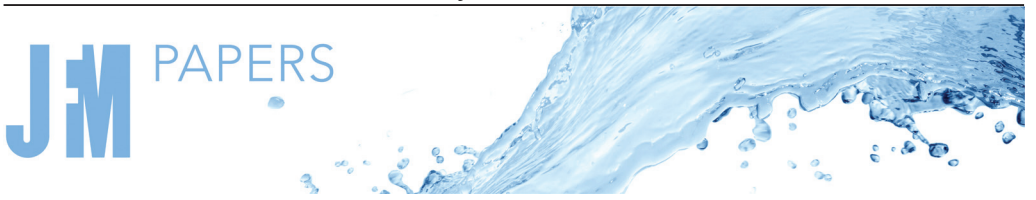

Mechanisms ruling the lifetimes of films of liquid mixtures

H.-P. Tran[1,2,3], N. Passade-Boupat[2,3,4], F. Lequeux[1,2,3] and L. Talini[5,†]

[1]CNRS, Sciences et Ingénierie de la Matière Molle, ESPCI Paris, PSL Research University, Sorbonne Université, 75005 Paris, France

[2]Laboratoire Physico-Chimie des Interfaces Complexes, ESPCI, 10 rue Vauquelin, 75005 Paris

[3]Laboratoire Physico-Chimie des Interfaces Complexes, Bâtiment CHEMSTARTUP, Route Départementale 817, 64170 Lacq, France

[4]Total S.A. 64170 Lacq, France

[5]CNRS, Surface du Verre et Interfaces, Saint-Gobain, 93300 Aubervilliers, France

(Received 26 November 2021; revised 3 June 2022; accepted 13 June 2022)

Foams and bubbles formed in liquid mixtures have lifetimes longer by several orders of magnitude than in pure liquids of similar viscosities. We have shown recently that this effect results from slight differences in molecular concentrations between bulk and surfaces, which give rise to a thickness-dependent surface tension of liquid films. We present a quantitative description of the enhanced stability of liquid films in binary mixtures, based on experimental data and theoretical analysis. Experiments were performed with mixtures of different natures and compositions: foams of stationary heights were obtained by continuous injection of gas, on one hand, and single bubbles were swollen under the surface of a liquid bath, on the other hand. Remarkably, the lifetimes measured in both experiments exhibit the same variations with mixture composition, and follow a power law with the microscopic length that characterises the amplitude of the thickness-dependent surface tension. In addition, the lifetimes vary with the squared film thicknesses at the onset of bursting. We suggest that two stages occur between the birth of liquid films and their rupture. We show how the thickness-dependent surface tension allows an equilibrium shape to be reached at the end of a first stretching stage. We give an analytical description of this shape, which is fully consistent with experimental findings. We suggest a possible mechanism for final rupture of the film, and discuss it in light of existing theoretical predictions. Finally, we compare the properties of liquid mixtures and surfactant solutions, and in particular their surface rheology.

Key words: foams, breakup/coalescence, thin films

† Email address for correspondence: laurence.talini@cnrs.fr

1. Introduction

Bubbles and foams formed in pure liquids are promised to a rapid death. As a result of either gravity or capillary suction by the curved parts they are connected to, liquid films thin down and there is no effect to oppose their drainage in pure liquids. Since their interfaces exert attractive van der Waals interactions upon one another, films quickly rupture when their thicknesses reach the range of these interactions, i.e. a few hundred nanometres. The duration of the latter process is very short, hence the lifetimes of liquid films mostly correspond to the drainage times, which expression depends on the effect driving drainage, i.e. capillarity or gravity (Debregeas, de Gennes & Brochard-Wyart 1998). Whatever the nature of the latter effect, the lifetimes of bubbles in pure liquids are at most a few tenths of milliseconds in liquids of water-like viscosities (Lhuissier & Villermaux 2012).

The case of bubbles or foams formed in surfactant solutions is more complex. At very small thicknesses, a repulsion between interfaces is induced by the adsorbed surfactants; the repulsion is of steric nature and may also result from charge interactions for ionic surfactants. Films in metastable states are thus observed, with lifetimes reaching hours (Rio & Biance 2014). In addition, drainage can be opposed by Marangoni effects, often described as a surface elasticity (Seiwert, Dollet & Cantat 2014) and resulting in a solid-like boundary condition at the interfaces. Surface viscous effects can as well come into play, resulting from e.g. finite adsorption times of surfactants (Scheid *et al.* 2010). The balance of the different effects at stake is expected to depend on surfactant concentration, and, accordingly, different behaviours are observed in moderately or concentrated solutions (Champougny *et al.* 2016) which adds to the complexity of the problem. Up to date, the precise mechanism of film rupture in surfactant solutions remains elusive. In addition, the link between the behaviours observed for single bubbles and those in foams is not clear.

A simpler – although poorly controlled – system is constituted by tap water, i.e. water containing surfactant species at vanishing concentrations. The interactions between the interfaces of liquid films are then expected to simply result from attractive van der Waals forces as in pure liquids; drainage of the liquid films can nevertheless be opposed by Marangoni effects as in surfactant solutions. Bubbles formed at the surface of a liquid bath were thus observed to last for seconds (Lhuissier & Villermaux 2012), i.e. their lifetimes are at least ten thousand times larger than the ones formed in pure liquids of similar viscosity, although the interactions between film interfaces are the same. A three-stage picture for the formation and rupture of the formed liquid film was suggested by Lhuissier and Villermaux. First, when a bubble rises to the surface of the bath, a liquid film is formed and stretched as a plug flow establishes. This stage is very fast, of similar duration as the drainage of films of pure liquids, i.e. of the order of 0.1 ms for water. As surfactant species are entrained by the flow from the apex to the foot of the bubble, a concentration gradient, and thus a surface tension gradient, is built. The end of this first stage is reached when the surface tension gradient is large enough to balance the effect causing drainage. An equilibrium is then reached for film tension; however, pressures are not in equilibrium since a pressure gradient persists as a result of capillary or gravity effects. A second stage then takes place, during which film drainage, driven by the pressure gradient, occurs. Unlike in the first stage, a solid-like boundary condition at the film interfaces is met, which results from the built surface tension gradient, and a Poiseuille flow establishes in the film. The drainage is therefore much slower in this second stage. Finally, the film further ruptures, by an unknown mechanism, which is very fast. As a result, bubble lifetimes are determined by the duration of the slowest second stage, which is orders of magnitude larger than the duration of the two other stages, and reaches seconds in tap water.

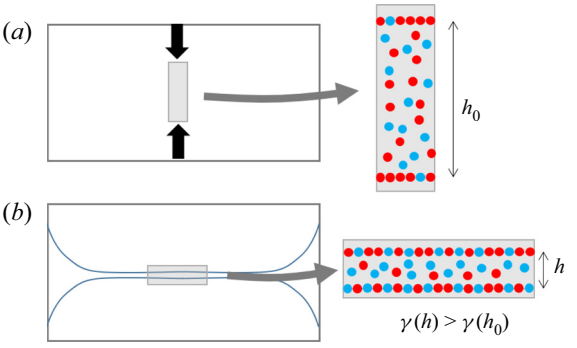

Figure 1. Illustration of the mechanism leading to increased surface tension when a film of liquid mixture is formed between two bubbles coming closer. The blue and red circles represent the two molecular species. The film is stretched at constant volume and, initially (*a*) its interfaces are enriched in the species with the lowest surface tension (red circles) compared with the bulk. Because the surface to volume ratio of the film increases during stretching, the surface and bulk concentrations of the different species cannot be kept constant. A new equilibrium is reached (*b*), in which the surface concentration of the red species is smaller than it was initially, resulting in a larger surface tension, which value depends on film thickness.

More controlled systems are constituted by mixtures of liquids. Foams and bubbles have been observed to last for a few seconds or even a few tens of seconds in low-viscosity mixtures (Ross & Nishioka 1975; Tran *et al.* 2020). In mixtures, the molecular interactions are the same attractive van der Waals forces as in pure liquids; in addition, long lifetimes have been observed with very different liquids, either polar or non-polar, either volatile or non-volatile, and are therefore unrelated to contamination by surfactant species or evaporation-induced Marangoni effects. Therefore, the enhanced stability of bubbles in mixtures cannot be understood by effects invoked in surfactant solutions or contaminated polar liquids. This has scarcely been discussed in the literature despite its practical importance. Actually, foaming of solvent mixtures can be detrimental in many processes of e.g. the oil industry, from crude oil extraction to car tank filling, or of the food industry where it is for instance observed in frying oils. As a matter of fact, addition of anti-foaming molecules is often required in the cited processes (Pugh 1996).

We have recently shown that the phenomenon at the origin of the longer bubble lifetimes in binary mixtures is the difference of molecular concentrations between the bulk and the interfaces, when the two liquids have different surface tensions (Tran *et al.* 2020, 2021). Actually, it has been established long ago that, in mixtures, the molecules with the smallest surface energy are more concentrated at the interface than in the bulk (Butler 1932; Prigogine & Marechal 1952; Eriksson 1964). We have demonstrated that the species with the lowest surface tension can thus play a surfactant-like role for the other species. Qualitatively, the effect we invoke is the following: when a foam forms, bubbles come closer to one another and liquid films between them are stretched, similarly to the first stage pictured for bubbles at the surface of tap water (Lhuissier & Villermaux 2012). This process is schematised in figure 1. Stretching at constant volume is associated with an increase of the surface to volume ratio and, if the concentrations of the two species composing the mixture are different in the bulk and at the interfaces, they cannot be kept constant because the film is not an infinite reservoir. Consequently, the interfacial concentration of molecules with the smallest surface energy decreases, resulting in a larger surface energy of the film. This effect can be described by a thickness-dependent surface tension of liquid films, characterised by a microscopic length α, as introduced

in our previous works (Tran *et al.* 2020, 2021). According to the picture described in figure 1, surface tensions of films increase when their thicknesses decrease. The resulting Marangoni-like effect is at the origin of the enhanced stability of foams formed in liquid mixtures.

The aim of the present work is to investigate the mechanisms determining the lifetimes of films of liquid mixtures, and in particular to gain insight into the relations between the different characteristic lengths at stake and the microscopic length α, which is linked to the partition of molecules between interfaces and the bulk.

The paper is organised as follows: in a second section, we detail the thickness-dependent surface tension of binary mixtures that has been established in our previous works. We further describe the experimental methods in § 3 and present experimental results on the lifetimes of foams and bubbles formed in liquid mixtures, as well as on the thickness of liquid films when they burst in § 4. Section 5 is devoted to the theoretical description and discussion of the rupture mechanism of liquid films in light of existing theoretical results. Finally, in § 6, we compare the stabilising effects of thin films formed in liquid mixtures with those of films formed in surfactant solutions.

2. Thickness-dependent surface tension of binary mixtures

In liquid mixtures, the partition of species between bulk and interface results in a surface tension of liquid films $\gamma(h)$ depending on film thickness h. The expression for $\gamma(h)$ is obtained by considering the creation of a liquid film from a given volume of liquid. Both initial and final configurations correspond to thermodynamical equilibria. In this volume, the initial number of moles is N_0 and the molar fractions are x_1^0 and x_2^0, the indices referring to the species composing the binary mixture. When the film is formed, N moles remain in the bulk while the interfaces with air are peopled with $(N_0 - N)$ moles. Since the surface and bulk concentrations differ, the bulk molar fractions change and become respectively x_1 and x_2. Writing the conservation equations of both species, both at the interfaces and in the bulk yields

$$x_1^0 - x_1 = \frac{N_0 - N}{N}(x_1 - X_1), \tag{2.1}$$

where X_1 is the molar fraction of species 1 at the surface.

Introducing the molar volume v and molar surface σ, assumed to be the same for both species, the ratio of the surface and volume of the film is $2/h = \sigma(N_0 - N)/vN$. The bulk molar fractions in the film depend on its thickness and the right-hand side of (2.1) can thus be written as $(x_1(h) - X_1)2v/\sigma h$. At the first order in $1/h$, it becomes $(x_1^0 - X_1)2v/\sigma h$, with the implicit notation $x_1^0 = x_1(\infty)$. The surface tension of the film can then be inferred from the expansion $\gamma(x_1) - \gamma(x_1^0) = (\partial\gamma/\partial x_1)(x_1 - x_1^0)$, where $\gamma(x_1)$ is the surface tension of a film of thickness h and bulk composition $x_1(h)$. Combining the latter relations, one obtains

$$\gamma(x_1(h)) = \gamma(x_1^0)\left(1 + \frac{\alpha}{h}\right) + O(h^{-2}), \tag{2.2}$$

where we have introduced the length α, which is characteristic of the mixture and depends on its bulk composition

$$\alpha = 2\left(\frac{\partial \ln\gamma}{\partial x_1}\right)_{x_1^0}(x_1^0 - X_1)\frac{v}{\sigma}. \tag{2.3}$$

Equation (2.2) describes the increase of surface tension in a thin film resulting from the concentration differences between bulk and surfaces. It is valid provided h remains larger

than molecular sizes. As discussed in previous works (Tran *et al.* 2020, 2021), the length α varies with mixture composition and reaches a maximum at a composition depending on the species at stake; its value is a few tenths of nanometres at most for the mixtures investigated herein. The length α also depends on the surfaces of the molecules at the interface, which are poorly known quantities since they are not measured but extrapolated from other properties (Eriksson 1964; Santos & Reis 2014). The value of α is particularly difficult to determine in mixtures of molecules of very different sizes. As a result, in the present work we limit our analysis to binary mixtures of molecules that have similar sizes, as assumed for the derivation of (2.3); in these symmetric binary mixtures, we have shown that the uncertainty on α is smaller (Tran *et al.* 2021). Finally, note that the thickness-dependent surface tension given by (2.2) can also be described in terms of surface elasticity. In § 6.1 we relate the length α to a Gibbs elastic modulus, which is a thickness-dependent quantity.

In (2.3), α is given as a function of both the surface molar fraction X_1 and the composition-dependent surface tension. Since the measurable quantity is surface tension, a relation between surface molar fraction and surface tension must be used in order to express α as a function only of surface tension. Several relations have been established and tested in the literature, but none of them accurately accounts for the experimental variations of surface tension. Among these approximate relations, the particularly simple Eberhart's law assumes a linear relation between surface tension and surface concentrations (Eberhart 1966) following: $\gamma(x_1^0) = \sigma X_1 \gamma_1 + \sigma X_2 \gamma_2$, where γ_1 and γ_2 are the surface tensions of respectively the species with the smallest and largest surface tension, $\gamma_2 > \gamma_1$. Further using the relation $X_1 + X_2 = 1$, a relation between $\gamma(x_1^0)$ and X_1 is obtained and (2.3) becomes

$$\alpha = 2\frac{v}{\sigma}\left(\frac{d\ln\gamma}{dx_1}\right)\left(x_1^0 - \frac{\gamma(x_1^0) - \gamma_2}{\gamma_1 - \gamma_2}\right). \tag{2.4}$$

Therefore, provided the molar volume and surface v and σ are known, the length α can be fully computed from the variations with composition of the surface tension of a mixture in an infinitely thick film, $\gamma(x_1^0)$.

In a mixture of molecules of similar sizes, the variations of surface tension with composition are sublinear, as a result of the molecular partition. Actually, because the species of smallest surface tension is more concentrated at the interface with air than in the bulk, the surface tension of the mixture is smaller than it would be for identical bulk and surface concentrations. The length α varies with the deviation of surface tension from linear behaviour, which is measured by the last term in parenthesis of the right-hand side of (2.4). An example of sublinear variation of surface tension with composition is shown in figure 2, together with the variations of α given by (2.4). The length α admits a maximum as emphasised above; it remains smaller than 0.1 nm in the chosen example. The values of α are necessarily approximate since, first, the same molar volume and surface are assumed for both species and second, the molar surface was inferred from the molar volume of one species (here octane), assuming cuboid molecules. In addition, Eberhart's law cannot accurately describe the variations of surface tension. We show in the following that, despite the absolute values of lengths α being approximate, their variations with composition strongly correlate with those of the bubble and foam lifetimes.

The relative variations of surface tension as a function of film thickness corresponding to the maximum value of α have been computed following (2.2) (inset of figure 2). Surface

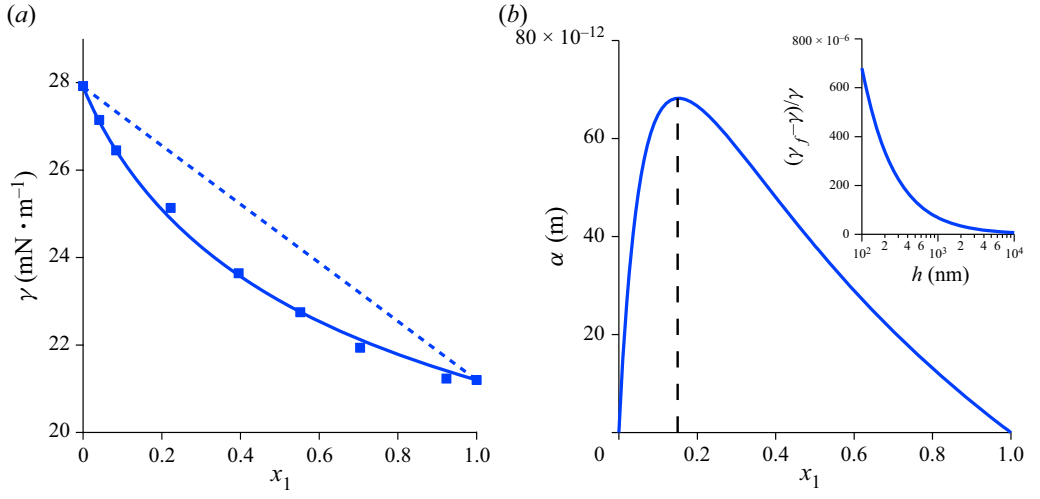

Figure 2. (*a*) Surface tension of a mixture of octane and toluene as a function of the molar fraction in octane. The full line is an interpolation of the experimental data (symbols). The dotted line indicates linear behaviour. (*b*) Corresponding variations with composition of length α computed from (2.4) with $v = 1.64 \times 10^{-4}$ m^3 mol^{-1} and $\sigma = 0.25 \times 10^6$ m^2 mol^{-1}. The relative variation of the thickness-dependent surface tension of a film of thickness h computed from (2.2) is shown in the inset for the maximum value of α indicated by the dashed line.

tension is larger at small thicknesses, but the relative increase of surface tension remains modest: it is smaller than 0.1% for a 100 nm-thick film in the chosen example. It reflects the small concentration differences between bulk and interfaces. This is why in figure 2 and in the following we have dropped the index 0, and we confound the molar fraction x_1^0 with x_1.

In summary, the partition of molecules between bulk and interfaces in liquid mixtures results in a larger surface tension in thinner films (provided their volume is constant) because of the finite number of molecules. The length α characterising the increase of surface tension is a submolecular length, an estimate of which can be provided from the variations of surface tension with composition of the mixture. Although the increase of surface tension is very small, we show in the following it is entirely at the origin of the enhanced stability of films formed in liquid mixtures, which lifetimes are approximately ten thousand times larger than those in pure liquids.

3. Experimental procedures

In the following, we describe the experiments performed either with foams or single bubbles formed in liquid mixtures.

3.1. *Liquid mixtures*

Both bubble rupture and foaming experiments have been systematically performed in three different liquid mixtures: octane-toluene, decane-toluene and heptanol-cyclopentanol. The properties of each liquid are reported in table 1. Their viscosities and surface tensions differ and so do the properties of their mixtures.

The surface tension of each mixture has been determined using a rising bubble tensiometer (Teclis). The density was obtained by assuming volume additivity, which

Liquid	Octane	Decane	Toluene	Heptanol	Cyclopentanol
γ(N m^{-1}) $\times$ 10^{-3}	21.6	23.8	28.5	26.2	32.7
μ(Pa s) $\times$ 10^{-3}	0.51	0.85	0.55	5.76	9.60

Table 1. Investigated liquids and their surface tension and viscosity values.

was checked to be valid. For each mixture, similar variations to the ones displayed in figure 2 for the octane-toluene mixture were obtained. The viscosities of the mixtures were determined as a function of composition by using the Kendall−Monroe relation (Kendall & Monroe 1917), which validity was tested by conducting viscosity measurements of selected mixtures. The variations of viscosity with composition are monotonic for all mixtures. In the following, data are shown for other alkane-toluene and alcohols mixtures than the three listed above. Their properties are fully detailed elsewhere (Tran *et al.* 2020).

3.2. *Foaming experiments*

Foams were formed by injecting gas (either nitrogen or air) at a controlled flow rate into a Bikerman column (Bikerman 1973), i.e. a cylindrical glass column at the bottom of which lies a porous filter (see figure 3). The column is first filled with a liquid mixture, and the conditions are such that, when gas is continuously injected, a foam forms with a stationary height. We emphasise that, at the same conditions, no measurable foam is observed in pure liquids in contrast to liquid mixtures. The foam lifetime in mixtures is defined from the measured stationary height of the foam, H, and gas velocity U

$$\tau = \frac{H}{U}. \tag{3.1}$$

It is independent of the gas velocity and of the initial liquid height in the investigated ranges. Measured lifetimes are at most a few tens of seconds.

We have found that evaporation modifies the lifetimes of foams. Experiments were performed in closed and open gas circuits: in the first case, a pump allows circulation of gas, which is quickly saturated with vapour of the binary mixture; in the second case, gas is injected in an open column and liquids continuously evaporate. As clearly shown in figure 3, significantly smaller lifetimes of foams are measured in the open circuit, in the presence of evaporation. This is consistent with the fact that faster evaporation of toluene (which is more volatile than decane) concentrates decane. A Marangoni effect may also be responsible for the smaller lifetimes: when the more volatile liquid has the largest surface tension, as in the used decane-toluene mixture, evaporation-induced Marangoni flows are expected to destabilise liquid films. In contrast, a stabilising Marangoni effect has been observed when the more volatile liquid has the smallest surface tension, as in water-ethanol mixtures (Hosoi & Bush 2001; Lorenceau & Rouyer 2020). We emphasise that, in contrast to other mixtures (Suja *et al.* 2018), in the systems investigated here, the enhanced stability of bubbles and foams cannot be attributed to Marangoni effects induced by evaporation since they are destabilising, and not stabilising, effects. We show in the following that the increased film lifetimes are fully accounted for by the thickness-dependent surface tension detailed in § 1. In order to probe the effect of mixture independently of evaporation-induced effects, all experiments were performed in a closed loop. The sizes of the bubbles in foams were measured and found to weakly vary with

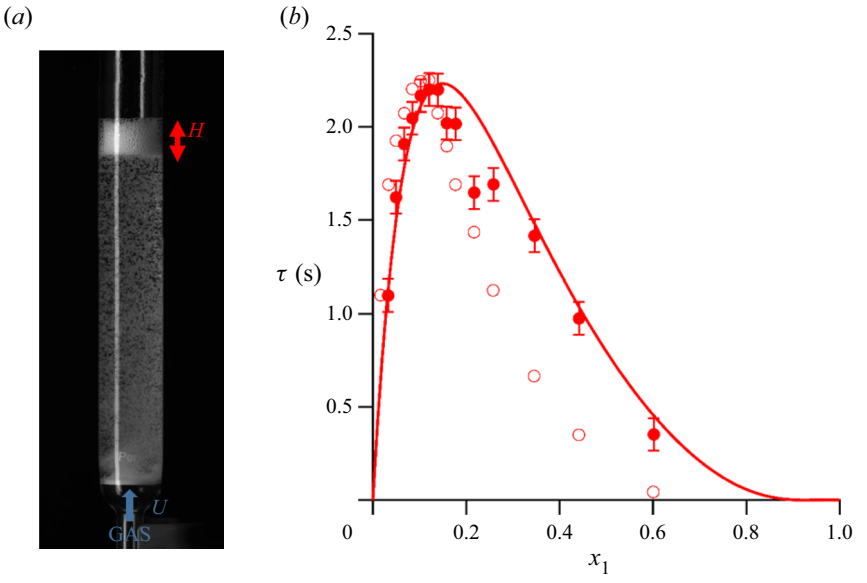

Figure 3. (*a*) Foam of stationary height H formed by continuous injection of gas at velocity U in a Bikerman column filled with a decane-toluene mixture. (*b*) Lifetime of the foam, as defined by (3.1), as a function of the molar fraction in decane. The experiment was performed in an open column (open circles) and in closed gas circulation (full symbols). The full line is a guide for the eye. For the sake of clarity, error bars (corresponding to the uncertainty on foam height) are shown for only one set of data.

height in the foam and from one liquid mixture to another. The average diameter is $2R_b = 1.6 \pm 0.3$ mm.

3.3. *Bursting bubbles*

Experiments in which single bubbles were swollen under the surface of liquid mixtures allowed measurements of two different parameters: first, the lifetime of bubbles, second, the thickness of the liquid film at the onset of bubble bursting. Air bubbles were formed at the tip of a tube immersed in a tank filled with liquid mixture. The dimensions of the tank were large compared with the size of the bubbles (diameter 2.5 mm). The bubbles were held at a distance of 1 mm from the free surface of the bath. They were imaged from the top at a frame rate of 37 500 f.p.s. and from the side at 30 f.p.s. As illustrated in figure 4, the top view allowed measurements of both bubble lifetimes and break-up kinetics. The side view was used to measure the bubble size and projection angle of the top view. The tank was covered by a lid in order to avoid significant evaporation.

Bubbles were swollen by injecting air at a constant flow rate. We have found that the swelling dynamics does not depend on air flow rate. Actually, the pressure in a bubble varies inversely with its radius of curvature and the latter does not vary monotonically: it exhibits a minimum when the droplet radius reaches the tube radius. As a result, pressure first increases until the bubble radius is that of the tube, and further decreases. Because of gas compressibility, the pressure drop is associated with air expansion in the whole circuit (syringe and tubing), which drives the kinetics of bubble expansion and make it independent of flow rate, in the conditions investigated herein.

Bubble lifetimes were measured from top views and defined as the time elapsed between the end of the swelling stage and bubble bursting. As illustrated in figure 5, which shows the cumulative distribution of bubble lifetimes measured over 50 different experiments

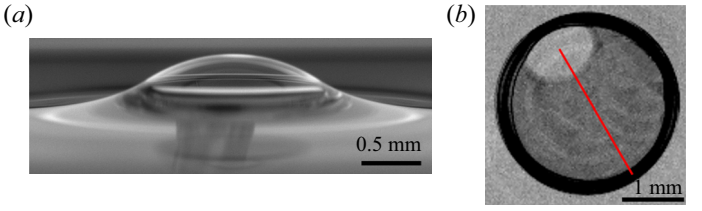

Figure 4. Side (*a*) and top (*b*) views of a bubble formed at the surface of a liquid bath. The bubble is formed at the tip of a tube at 1 mm from the liquid surface. The side view allows measurements of lifetimes and geometrical parameters of the bubbles. The velocity of hole opening is measured from space vs. time diagrams built from profile measurements along the shown line on the top view.

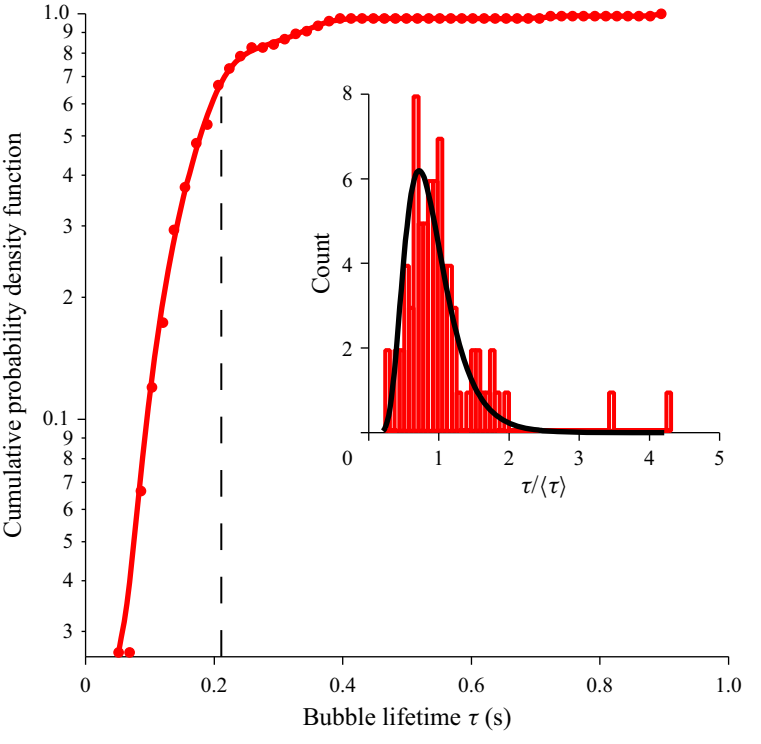

Figure 5. Cumulative probability density function of bubble lifetimes measured at the surface of a liquid mixture (decane-toluene, $x_1 = 0.12$). The result of 50 different experiments is shown and the dotted line indicates the average value of bubble lifetime. Inset: corresponding histogram of bubble lifetimes, normalised by their average value. The full line is a fit to the data by a log–normal distribution.

in decane-toluene mixtures, the distributions are close to log–normal distributions with a maximum reached at a value close to $\langle\tau\rangle$, which is the average lifetime. In other mixtures, the lifetimes were averaged over 25 experiments for each set of experimental conditions. Since all distributions were fairly described by log–normal distributions, in the following, we consider that the uncertainty on the average lifetime is very small and do not show error bars on the corresponding data.

Bubbles were found to puncture at a reproducible location, corresponding to a radius making an angle of $26 \pm 3^\circ$ with respect to the vertical axis. No significant differences in angles were observed between the different mixtures nor between different compositions

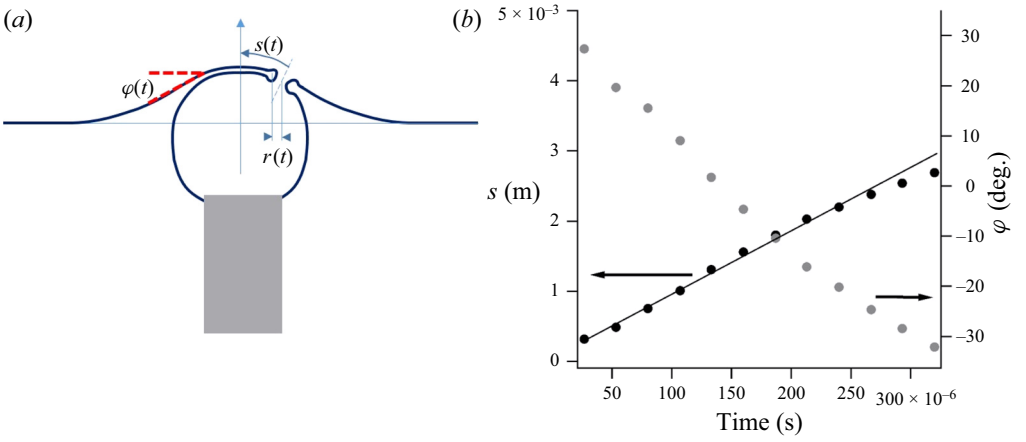

Figure 6. (*a*) Scheme of a bursting bubble. The curvilinear length travelled by the edge of the opening hole, $s(t)$, and the angle $\varphi(t)$ are obtained from the projection $r(t)$ in the horizontal plane measured from top views of the bubble. (*b*) Variations with time of distance s (left axis, black circles) and angle φ (right axis, grey circles). Data obtained with a heptanol-cyclopentantol mixture of heptanol molar fraction $x_1 = 0.12$. The slope of the full line is the Taylor–Culick velocity from which the thickness at bursting is inferred.

of the same mixture. Interestingly, in pure viscous oils, bubbles were observed to puncture at the apex (Debregeas *et al.* 1998), similarly to bubbles formed in concentrated (i.e. above the critical micellar concentration) aqueous surfactant solutions (Champougny *et al.* 2016). In contrast, holes open close to the foot when the liquid is either a low concentration surfactant solution (Champougny *et al.* 2016) or tap water (Lhuissier & Villermaux 2012). Remarkably, the bursting locations in fluid mixtures are similar to the ones reported in moderately concentrated surfactant solutions.

We have investigated the kinetics of hole opening when bubbles burst. The curvilinear distance travelled by the edge of the opening hole, $s(t)$, is obtained from analysis of top view images. As shown in figure 6, the hole opens at constant velocity during a first stage, after which the velocity slightly decreases. The first stage ends when the hole extends beyond the bubble apex (corresponding to $\varphi = 0$ in figure 6). The observed kinetics reveals that, at the onset of bursting, the liquid film has a homogeneous thickness, which is indicative of negligible drainage occurring before bursting.

The film thickness is determined by using the Taylor–Culick relation between the hole-opening velocity v and the film thickness h_b at bursting (Culick 1960)

$$h_b = \frac{2\gamma}{\rho v^2}, \tag{3.2}$$

where ρ is the liquid density and γ its surface tension.

The resulting thicknesses are in the micron range, and depend on the nature of the mixture and its composition. The thickness values that are reported in the following are those found at the first and constant-velocity stage of hole opening, and thus correspond to the homogeneous thickness of the film when it punctures.

In summary, we have measured the lifetimes of both singles bubbles and foams formed in liquid mixtures. Although the bubble radius R_b is larger in single bubble experiments, the Bond number that compares gravity and capillarity, $Bo = \rho g R_b^2/\gamma$, remains smaller than unity, $Bo \approx 0.5$. As a result, the liquid films are destabilised by capillary suction in both foam and bubble experiments; therefore, the same physical effect is probed in both

experiments, although the lifetimes differ. The distinct values of the lifetimes result from differences in the geometry of liquid films.

4. Experimental scaling laws

4.1. *Measured characteristic lengths*

In order to compare lifetimes measured in liquid mixtures of different compositions, and to account for the differences in viscosities and surface tensions, we introduce a length L

$$L = \tau V^*, \tag{4.1}$$

where τ is the lifetime (either of bubbles or foams) measured in a mixture and V^* is the capillary velocity in the same mixture, $V^* = \gamma/\mu$.

In liquid mixtures, the length L is much larger than the other characteristic lengths of the problem: it ranges from a few to a hundred metres. These strikingly large values can be understood by considering that, in pure liquids, the lifetimes of liquid films emptying by capillary drainage are expected to scale as R_f/V^*, R_f being the radius of curvature of the meniscus (or the Plateau border in a foam). As emphasised by Lhuissier and Villermaux, it is equivalent to the drainage time $\mu/\rho g R_f$ measured at large Bond numbers in silicone oils when gravity drives drainage (Debregeas *et al.* 1998). As a result, in pure liquids, the length L defined by (4.1) is of the same order of magnitude as R_f, i.e. millimetric. In contrast, in the mixtures we consider, the lifetimes are larger than in pure liquids by approximately ten thousand times and the lengths L are consequently larger than R_f by the same numerical factor, reaching tens of metres. The giant lengths L we measure therefore simply reflect the enhanced stability of liquid films in liquid mixtures compared with pure liquids.

We report in figure 7 the variations of L obtained from the measured lifetimes of bubbles and foams in the different mixtures as a function of their compositions. As for lifetimes, a maximum is found for L in each nature of mixture. Interestingly, the values of the lengths L determined in single bubble experiments are smaller by one order of magnitude than the lengths obtained in foaming experiments. In both experiments, liquid films are connected to a curved meniscus and drain. However, the curvature of the meniscus differs: whereas it is given by the capillary length for single bubbles at the surface of a liquid bath, it depends on the size of the bubbles and on the liquid fraction in foams (Cantat *et al.* 2013). In the foams we consider, we roughly estimate the average liquid fraction to be close to 10 % and thus the radius of curvature of the Plateau border to be approximately half the bubble radius, i.e. close to 500 μm (Cantat *et al.* 2013), which is smaller than the capillary length. We emphasise this value is approximate and, in particular, is not expected to be constant over the foam height, because of gravity-induced drainage. As a result, it is difficult to precisely account for the role of the curvature of the Plateau border in foams.

Although the absolute values of L are different in single bubble and foam experiments, figure 7 shows that their relative variations with composition are nevertheless remarkably similar. This similarity demonstrates that the lifetimes of foams and of single bubbles at free surfaces are determined by the same mechanisms. The distinct values of L simply reflect the geometrical differences in both experiments, as emphasised above. In the following, we suggest a unified picture of the mechanisms ruling the lifetimes in both experiments.

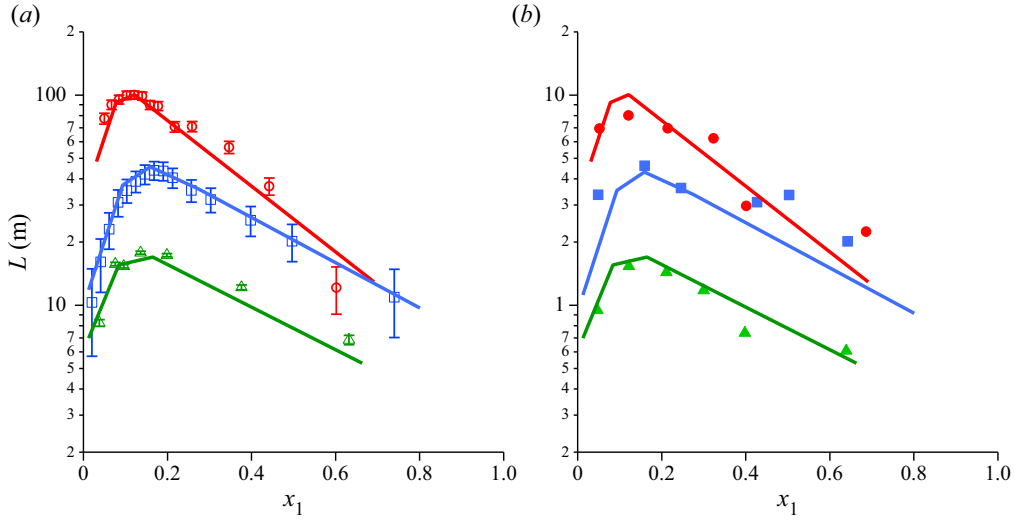

Figure 7. Characteristic lengths defined as the products of lifetimes and capillary velocities as a function of the molar fraction in the mixture of the species with the smallest surface tension. Results of (*a*) foaming experiments and (*b*) single bubble experiments are shown in mixtures of decane and toluene (red circles), octane and toluene (blue squares) and heptanol and cyclopentanol (green triangles). The error bars in (*a*) result from the uncertainty on foam height. The lifetimes of single bubbles were averaged over 25 experiments performed at the same conditions. The same guides to the eye (full lines) are shown in each graph, vertically translated to account for the different scales of the vertical axes.

4.2. *Experimental scaling of length L with length α*

In each mixture, the length α characterising the thickness dependence of surface tension can be computed as a function of concentration, and compared with the variations of length L. An example is shown for octane-toluene mixtures in figure 8, in which the variations of α and L are plotted on the same graph. Because of the very different orders of magnitude of these lengths (tens of picometres vs. tens of metres), two axes are used but, remarkably, their variations are described by the same curves. Clearly, there is a proportionality relation between these lengths and the thickness-dependent surface tension is the leading effect determining the lifetimes of foams and bubbles.

To further support this view, we report experimental data in different alkane-toluene and alcohol mixtures than the ones specified above, and on which details can be found elsewhere (Tran *et al.* 2020). As pointed out above, the absolute value of α is poorly determined, in particular in the case of mixtures of molecules with very different sizes; as a result, herein, we focus on molecules rather symmetric in sizes. Figure 8(*b*) shows L as a function of α for these symmetric mixtures and both lengths are normalised by their maximum value.

Although the data are rather scattered, they nonetheless confirm the linear increase of length L with α. We attribute data dispersion to the poor determination of the absolute values of α. In particular, the molar surfaces that are needed to compute α were obtained from molar volumes in the cuboid-molecule approximation. In what follows, we compare L with another parameter, which is directly determined in single bubble experiments, namely h_b, the film thickness at the onset of bursting.

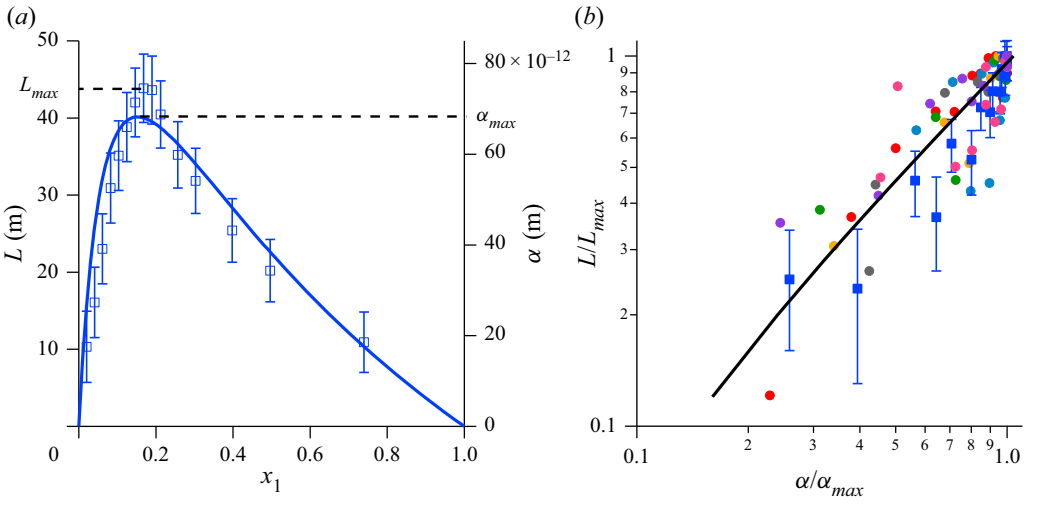

Figure 8. (*a*) Lengths L (symbols, left axis) and α (full line, right axis) as a function of composition of octane-toluene mixtures. Here, L was measured in foaming experiments and α was computed from the experimental composition dependence of surface tension using (2.4). The maximum values L_{max} and α_{max} are reached for the same composition. (*b*) Normalised length L as a function of the normalised length α for eight different liquid mixtures. Both L and α are normalised by their maximum values found in each mixture at a given composition. The full line is a guide for the eye indicating a linear increase.

4.3. *Experimental scaling of length L with thickness at bursting*

As detailed above, we have conducted measurements of the liquid film thickness when a bubble punctures. From the measured hole-opening velocity that follows the Taylor–Culick relation given by (3.2), we have found that bursting occurs at a very reproducible film thickness, which is, in addition, spatially homogeneous. This thickness ranges from approximately 500 nm to a few microns, according to the liquid mixture. The experimental range is the same as observed e.g. in tap water (Lhuissier & Villermaux 2012). Figure 9 shows the variations of length L with thickness h_b for three different liquid mixtures. The length L spans almost one decade and its variations with thickness follow a power law with an exponent 2.

In summary, a length L ranging from metres to 100 m is defined from the measured lifetimes of foams and single bubbles formed in liquid mixtures, its large value reflecting the strong increase of lifetimes compared with those in pure liquids. The variations of L with mixture composition are the same in both foaming and single bubble experiments, showing the same effects are at stake in the rupture of liquid films despite geometrical differences. In addition, we have measured the thickness of liquid films at the onset of bubble bursting; remarkably, this thickness is spatially homogeneous. The length L has been compared with the microscopic length α that characterises the thickness dependence of surface tension in mixtures, resulting from the finite reservoir effect; α can be computed from the variations of surface tension of a mixture with its composition, provided an assumption is made for molecular surfaces. We have found the variations of these two lengths with composition follow the same curve, thus establishing the experimental scaling law verified with a large selection of mixtures of either polar or non-polar liquids

$$L \propto \alpha. \tag{4.2}$$

In addition, the thickness at rupture of the liquid film has been determined to be larger than 500 nm and the variations of L with the latter thickness have been found to follow the

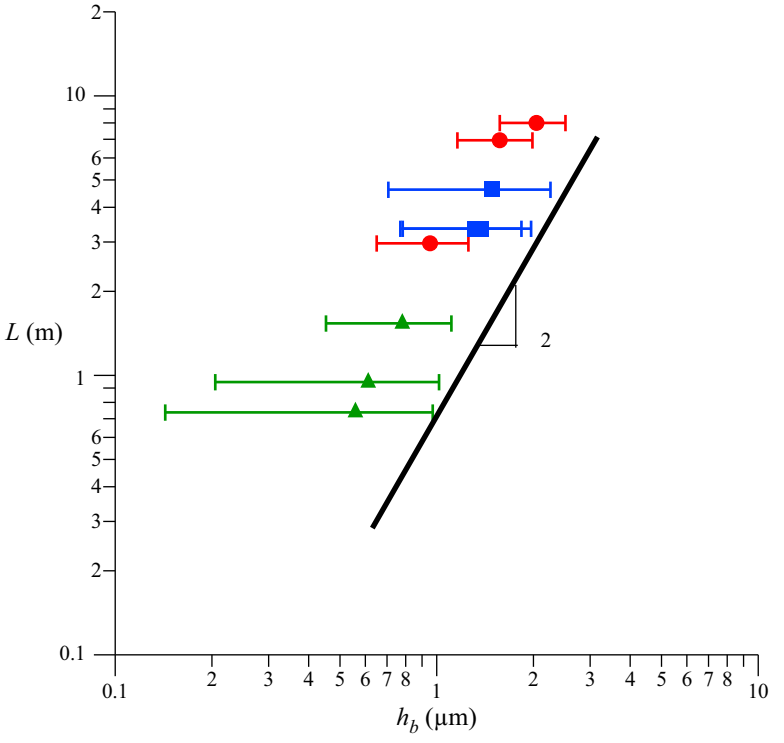

Figure 9. Length L as a function of film thickness at bursting, both measured in single bubble experiments performed with mixtures of decane and toluene (red circles), octane and toluene (blue squares) and heptanol and cyclopentanol (green triangles). Thickness h_b is determined from measurements of Taylor–Culick's velocity using (3.2), error bars on h_b result from the uncertainty on Taylor–Culick's velocity.

scaling law $L \propto h_b^2$. Therefore, using (4.2), the following scaling law can be inferred:

$$h_b \propto \alpha^{1/2}. \tag{4.3}$$

In the following theoretical section, we analyse the effect of the thickness-dependent surface tension on thin films and we further discuss the possible mechanisms driving film bursting and the expected scaling laws.

5. Theoretical analysis and discussion

5.1. *Tension equilibrium before drainage*

As explained above, two stages can be considered before film rupture: in a first stage, a film forms between two bubbles by stretching until a mechanical equilibrium is reached; in a second stage, the film drains because of the pressure difference between its flat and curved parts. This picture is relevant provided the duration of the drainage stage is much larger than the time needed for film formation. We will come back to this point later. We first write the mechanical equilibrium for the film considered as a whole (bulk and interfaces). We emphasise an equilibrium is reached for film tension but not for pressure. The pressure gradient driving drainage will be discussed in the next section. In the analysis that follows, we neglect the effect of intermolecular forces, i.e. the disjoining pressure term. As explained below, its influence is limited to the very final stage of the film.

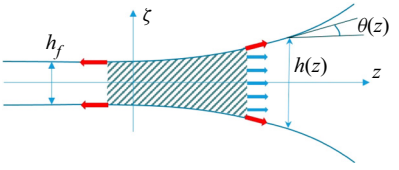

Figure 10. Scheme of a liquid film and equilibrium of its whole tension on a part of the film (hatched area). The red arrows represent the contribution of surface tension and the blue arrows the net force resulting from the sum of pressure forces.

We now consider a part of the film, such as that schematised in figure 10, and the forces it is submitted to. The net pressure force $\oint P\,\overrightarrow{\mathrm{d}s}$ exerted on the surface of the element considered simply results in the Laplace pressure: actually, the constant pressure term vanishes because $\oint \overrightarrow{\mathrm{d}s} = \vec{0}$ for any closed surface. Therefore, the forces exerted on a film in the z-direction (per unit length in the direction perpendicular to the plane) consists of interfacial tension and of the product of the Laplace pressure in the liquid and local thickness. We refer to the sum of these forces by unit length as the film tension, which differs from interfacial tension. At equilibrium, the film tension is constant, yielding

$$2\gamma(h)\cos(\theta(z)) + h(z)\Delta P(h) = \text{const.}, \tag{5.1}$$

with $\theta(z)$ the local angle of the film surface with the z-direction at z and ΔP the Laplace pressure.

The increased surface tension $\gamma(h)$ in the thin part of the film therefore allows an equilibrium to be reached for film tension. We emphasise the same equation can be obtained by minimising the free energy of the system given by $\int 2\gamma(z)\sqrt{1+(\partial(h/2)/\partial z)^2}\,\mathrm{d}z$. In addition, (5.1) is similar to the one established for soap films ((106) in Ivanov 1988). In the latter case, however, equilibrium is not ensured by a thickness-dependent surface tension but by disjoining pressure.

Going back to (5.1), we limit our analysis to small curvatures (for the sake of simplicity) and therefore the Laplace pressure is simply given by $\Delta P(h) \cong \gamma(h)\partial^2(h/2)/\partial z^2$. In addition, for small angles, we use $\cos(\theta(h)) \cong 1 - (\partial(h/2)/\partial z)^2/2$. The constant in (5.1) is determined by considering the tension of the film in its flat part. As the reference for pressure is that in the gas phase, and because we do not consider the effect of disjoining pressure, the film tension in the flat part of thickness h_f (see figure 10) is simply $2\gamma(1+\alpha/h_f)$. Equation (5.1) finally becomes

$$\gamma\left(1+\frac{\alpha}{h}\right)\left(2-\frac{1}{4}\left(\frac{\partial h}{\partial z}\right)^2+h\frac{\partial^2 h}{2\partial z^2}\right)=2\gamma\left(1+\frac{\alpha}{h_f}\right). \tag{5.2}$$

We introduce the dimensionless variables $H(\xi) = h(z)/h_f$ and $\xi = z/w$, where w is an unknown characteristic length in the z-direction. We also introduce the dimensionless number $Y = \alpha/h_f$. In practice, $Y \ll 10^{-3}$, as will be shown in the following. Expanding (5.2) in Y leads at first order to

$$\frac{4Yw^2}{h_F^2}\left(\frac{1}{H}-1\right)+\left(-\frac{1}{2}H'^2+HH''\right)+O(Y^2)=0. \tag{5.3}$$

We emphasise that, for $Y = 0$, i.e. a constant surface tension, (5.3) is the simple equation of pressure equilibrium in the film. The only solution is then $H = a(\xi - b)^2$ where a and

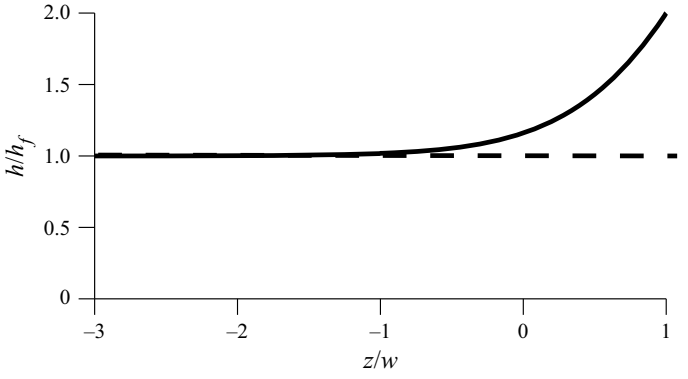

Figure 11. Profile of the interface of a liquid film in mechanical equilibrium given by (5.6) with $H = 2$ for $\xi = 1$.

b are constants. However, this parabolic solution cannot connect a flat film with a Plateau border and is therefore not physically sound. As a result, a relevant solution to (5.3) can be found only if the surface tension is thickness dependent.

A natural value of lateral length is $w = h_f Y^{-1/2} = h_f^{3/2}/\alpha^{1/2}$. Equation (5.3) can then be solved by using H as a variable. We denote $\Theta(H) = (\mathrm{d}H/\mathrm{d}\xi)/2$ the dimensionless slope of the interface. Therefore, $H'' = 2\Theta'\,\mathrm{d}H/\mathrm{d}\xi = 4\Theta\Theta'$, and (5.3) becomes, if expressed as a function of the variable H

$$\left(\frac{1}{H} - 1\right) - \frac{\Theta(H)^2}{2} + H\Theta(H)\Theta'(H) = 0. \tag{5.4}$$

The general solution to (5.4) is $\Theta = \sqrt{1 - 2H + H^2 k}/\sqrt{H}$ where the constant k remains to be determined. The value of k is such that Θ tends toward zero when H tends toward unity, which yields $k = 1$. A solution connecting a flat film and a Plateau border can therefore be found provided the surface tension is thickness dependent. This solution is given by

$$\Theta = \frac{H - 1}{\sqrt{H}}. \tag{5.5}$$

Equation (5.5) is an implicit equation, and the explicit inverse function of the solution can be obtained by integration with respect to ξ

$$\sqrt{H} + \frac{1}{2}\mathrm{Log}\left(3 - \frac{6}{\sqrt{H} + 1}\right) = \xi - c, \tag{5.6}$$

where c is an integration constant.

We arbitrarily choose $H = 2$ for $\xi = 1$. The corresponding variations of $h(z)/h_f$ as a function of the dimensionless position are shown in figure 11.

As expected, the curvature of the meniscus, $h''/2$ tends toward a constant value for large thicknesses, and this value corresponds to either the curvature of the Plateau border in a foam, or that of the meniscus for a single bubble. We denote the curvature as $1/R_f$,

which yields

$$\mathrm{Lim}_{z\to\infty}\frac{h''}{2}=\frac{h_f}{w^2}=\frac{1}{R_f}. \tag{5.7}$$

Combining (5.7) and $w=h_f^{3/2}/\alpha^{1/2}$ gives the relations

$$h_f=\alpha^{1/2}R_f^{1/2}, \tag{5.8}$$

and

$$w=\alpha^{1/4}R_f^{3/4}. \tag{5.9}$$

At equilibrium, i.e. after the stretching stage and before significant drainage, the film thickness and the characteristic lateral length are therefore functions only of the radius of the Plateau border and of the microscopic length α; the latter characterises the concentration differences between bulk and surface in the liquid mixture. Since α is subnanometric and R_f is millimetric, the thickness of the film at equilibrium is within the micron range, and the lateral length is roughly ten times larger. Importantly, w is two orders of magnitude smaller than the radius of the Plateau border. For instance, for $\alpha=0.1$ nm and $R_f=1$ mm, the lateral length and thickness at equilibrium are respectively $w\cong 20$ μm and $h_f\cong 300$ nm.

The scaling law $h_f\propto\alpha^{1/2}$ is the same as the one experimentally determined for thickness at bursting, h_b. In the following, we suggest that these thicknesses are confounded, i.e. that, when it drains, the film keeps its equilibrium thickness everywhere but in a very localised part that pinches.

5.2. *Dynamics of pinching*

The previous analysis provides the shape of a film at the end of the stretching process and before it drains. As emphasised above, pressure in the flat part of the film is larger than in its curved part. Because of the non-zero pressure gradient, the film is expected to thin down at some location, forming a pinch, during this stage (Aradian, Raphael & de Gennes 2001). Pinching occurs provided the interfaces are rigid, i.e. a zero-velocity condition is verified. The suggested scenario ending by film bursting is that, as the pinched part further thins down, a critical thickness is reached for which van der Waals attraction becomes effective (Chatzigiannakis & Vermant 2020; Shah *et al.* 2021); the film then pierces very quickly. The film lifetime is therefore given mostly by the time needed for the pinched part to reach the critical thickness, which is much larger than both the durations of the first stretching stage and of the last piercing stage under the action of van der Waals forces. In the following, we discuss the pinching dynamics liquid films formed in liquid mixtures.

In the previous section, we have discussed the effect of stretching only, because stretching and drainage are decoupled stages of the film lifetime. More precisely, in the lubrication approximation, the velocity v of liquid in the bulk of the film is parabolic and, without loss of generality, can be expressed as

$$v(z,\zeta)=V(z)+A(z)\left(\zeta+\frac{h}{2}\right)\left(\zeta-\frac{h}{2}\right), \tag{5.10}$$

where ζ is the coordinate in the direction normal to the interfaces of the flat film (see figure 10). We have assumed in (5.10) that the z-axis is a symmetry axis. Here, $V(z)$ corresponds to a plug flow, while the second term of the right-hand side corresponds to

a Poiseuille flow, with a condition of vanishing velocity at the interfaces, for $\zeta = \pm h/2$. Also, $A(z)$ depends on the pressure gradient.

The equilibrium of tension discussed above and leading to (5.2) corresponds to the condition $V = 0$, reached at the end of the stretching stage. Therefore, if surface tension is not modified by drainage, the condition $V = 0$ remains true as fluid drains, and the flow is a Poiseuille flow with a zero-velocity condition at the interfaces. We show in the following that this is the case at the pinch because the concentrations are not modified.

Drainage in a liquid film may indeed induce changes in the local concentration of the mixture. For instance, drainage from a thin film part to a thicker part will increase the concentration of the species of lowest surface energy in the thicker part, and thus decrease surface tension. However, when liquid is only expelled and not renewed at some place, bulk concentrations are not modified even if the film thickness locally changes at this place; as a result, the equilibrium between bulk and interfaces is not modified and neither is surface tension. Thus, in the regions of the films from which liquid flows, surface tension does not vary and does not depend any more on thickness. This is likely the case at the pinch location, where most of the liquid is drained towards the Plateau border, whereas the incoming flow is negligible if the thickness of the other parts of the film does not vary. Because the tension of the film is in equilibrium before pinching, and as long as the curvature at the pinch is small compared with that of the Plateau border, the zero-velocity condition at the interfaces remains valid. In this approximation, pinching of the film may be described by the solution given in the literature (Aradian *et al.* 2001). Applying this solution to our problem, and assuming the thickness of the flat film is h_f, we obtain for the thinning dynamics at the pinch

$$h(t) \cong \frac{R_f h_f^{1/2}}{V^{*1/2} t^{1/2}}, \tag{5.11}$$

where, for the sake of simplicity, the numerical prefactor is not given.

In this picture, the pinch thins down following (5.11) until it reaches a thickness h_{vdw} at which van der Waals attraction accelerates thinning. An estimate of the film lifetime is obtained by assuming the latter stage is very rapid and that lifetime is mostly given by the time to reach the thickness h_{vdw}, yielding from (5.8) and (5.11)

$$L \cong \frac{h_f R_f^2}{h_{vW}^2} \cong \frac{\alpha^{1/2} R_f^{5/2}}{h_{vW}^2}. \tag{5.12}$$

The resulting scaling law $L \propto \alpha^{1/2}$ is in discrepancy with our experimental finding $L \propto \alpha$. As emphasised above, the final stage of thinning under the action of van der Waals forces is not taken into account in the description leading to (5.12). The effect of van der Waals attraction on the pinching dynamics has been recently discussed in detail in the literature (Shah *et al.* 2021). On the basis of the corresponding numerical results, an exponent 5/14 instead of 1/2 is expected for α in (5.12) when the final stage is accounted for. The exponent is thus slightly smaller and this effect cannot explain the disagreement with our experimental observations. We suggest instead that two-dimensional flows may be involved during pinching, requiring a new analysis for the dynamics of pinch thinning. This picture is supported by experimental reports that pinches forming at the foot of bubbles further exhibit complex dynamics (Frostad *et al.* 2016) (see the videos in supplemental information).

Basically, the only lengths involved in the problem are α, h_{vW} and R_f. Because we observe that L is proportional to α, we suggest the following phenomenological law

$$L \sim \alpha \left(\frac{R_f}{h_{vW}} \right)^a. \tag{5.13}$$

The order of magnitude of L is consistent with an exponent $a = 3 \pm 0.5$, but obviously, complementary experiments are required for further insight into this analysis.

In summary, we have shown that surface tension of liquid mixtures is thickness dependent, which introduces a new length α making the problem of film formation and bursting very rich, with length scales ranging from molecular sizes to tens of metres. Taking advantage of the − relatively − simpler situation faced in liquid mixtures compared with surfactant solutions, an analytical solution is found for the equilibrium shape reached by liquid films at the end of a stretching stage. In agreement with experimental scaling laws, we suggest liquid films further keep their equilibrium thickness while a localised pinching is responsible for their rupture. Dynamics of the pinched part remains to be determined. It is indeed tempting to compare the picture of the fate of liquid films we have established in liquid mixtures with that of the widely studied soap films, i.e. made from aqueous surfactant solutions.

6. Comparison with soap films

Films of surfactant solutions differ from films of liquid mixtures in two ways. First, whereas the forces between the interfaces of films of mixtures are purely attractive, those in soap films have a repulsive component. According to the nature of surfactants, the latter repulsion may originate from steric or electrostatic effects; it allows films to reach metastable states at small thicknesses (100 nm and below), and to last for very long times. In contrast, as shown above, films of liquid mixtures, which interfaces have purely attractive interactions, have much smaller lifetimes and break at much larger thicknesses. The second difference is that the exchange kinetics between bulk and interfaces is much slower in the case of surfactants. Whereas molecular diffusion homogenises a 1 µm-thick film of liquid mixture in less than 1 ms, adsorption of surfactants at the interfaces of soap films can take up to tens of seconds. In the following, we underline the analogies between films of surfactant solutions and liquid mixtures.

6.1. *Gibbs elasticity*

The effect we describe in liquid mixtures is analogous to the Gibbs elasticity in surfactant solutions. Actually, extension of a soap film is opposed by the induced surface tension gradients, resulting in a surface elastic modulus $E = -2\,\mathrm{d}\gamma/\mathrm{d}\ln h$. As in liquid mixtures, the associated surface elastic modulus is found by writing conservation of mass (Gibbs 1961; van den Tempel, Lucassen & Lucassen 1965), which yields, provided the Gibbs adsorption isotherm is verified

$$E = \frac{4\Gamma^2}{c} RT \frac{1}{h + 2\frac{\mathrm{d}\Gamma}{\mathrm{d}c}}, \tag{6.1}$$

where Γ and c are respectively the surface and bulk concentrations in surfactant, R is the ideal gas constant and T is the absolute temperature.

Gibbs moduli of surfactant solutions therefore depend upon film thickness, which is rarely considered in the literature but has been evidenced experimentally (Prins, Arcuri &

Vandente 1967). According to (6.1), in the limit $h \gg \mathrm{d}\Gamma/\mathrm{d}c$ the modulus verifies $E \propto h^{-1}$. Since $\mathrm{d}\Gamma/\mathrm{d}c$ is a molecular length, this limit is generally reached.

By analogy, it is straightforward to derive the surface elastic modulus of liquid mixtures from the thickness-dependent surface tension given by (2.2)

$$E = 2\gamma\frac{\alpha}{h}. \tag{6.2}$$

The surface elastic modulus of a liquid mixture is therefore of the order of a few tenths of mN m^{-1} for a 10 nm-thick film and $\alpha = 0.1$ nm. Similar values were obtained with surfactant solutions, although the thickness dependency of E was not taken into account (Champougny *et al.* 2015). We emphasise that there is a strong analogy of the effects at stake in surfactant solutions and liquid mixtures. Along this line, we show in the Appendix A that a similar length α can be defined in surfactant solutions. Nevertheless, the surface rheology of liquid mixtures is much simpler than those of surfactant solutions in which adsorption times at the interfaces may induce significant surface viscosities (Scheid *et al.* 2010). In contrast, in the liquids we consider, the equilibrium times are those for molecular diffusion and surface viscosity can be neglected. The understanding of thin film behaviour in liquid mixtures can therefore provide new insight into the role of surface elasticity, decoupled from other rheological effects. In the following, we analyse the differences that can be expected during film formation.

6.2. *Regimes of film formation*

Thus far, we have assumed that film formation and drainage are decoupled stages of the life of a liquid film. Obviously, this description fails if the duration of film formation is of the same order as that of drainage. We discuss in the following the mechanism of film formation in both limits, i.e. stretching with negligible drainage and drainage without stretching. The latter limit has been widely discussed in the literature, in light of the analogous problem of the formation of soap films from a reservoir (Mysels, Shinoda & Frankel 1959; Seiwert *et al.* 2014).

Mysels, Shinoda and Frankel (Mysels *et al.* 1959) solved the problem of soap film entrainment by a solid frame from a reservoir in the case of an incompressible interface. They predicted that the resulting film thickness follows a power law with the velocity at which the film is pulled from the reservoir. In some of the experiments that have been conducted since in aqueous surfactant solutions, deviations from the predicted law were observed, which were attributed to surface elasticity or viscoelasticity (Scheid *et al.* 2010; Seiwert *et al.* 2014). For an incompressible interface, Frankel's law expresses the thickness of a film as a function of the pulling velocity V (Mysels *et al.* 1959)

$$h_{Fr} = 2.68l\left(\frac{V}{V^*}\right)^{2/3}, \tag{6.3}$$

where l is the characteristic length of the problem, similar to the Plateau border curvature. We can compare the thickness predicted by (6.3) with the thickness we predict in the absence of drainage. Depending on the physicochemical parameters and on the velocity of the film formation, two situations, which are represented in figure 12, are encountered.

- $h_f \gg h_{Fr}$. In that case the stretching equilibrium cannot been reached since drainage efficiently thins the film down. As a result, the film formation is governed by drainage, and its thickness is h_{Fr}.

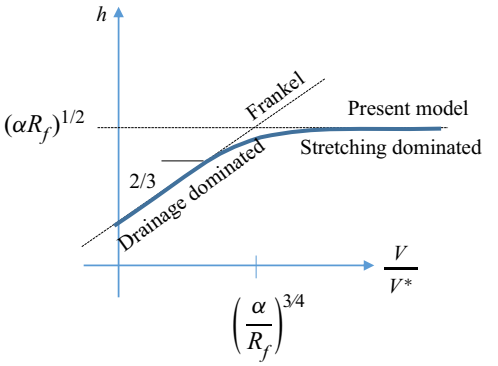

Figure 12. Thickness of a film of liquid mixture according to the velocity at which it is formed. At low velocities, drainage prevails over stretching and the thickness follows Frankel's law. At larger velocities, the film is stretched without significant drainage, and its thickness reaches a plateau value depending on both the radius of its curved part and the molecular length α.The regime examined herein is the high-velocity one.

- $h_{Fr} \gg h_f$. In that case, drainage would lead to a film thickness larger than that of the stretching mode. Film formation is therefore governed by stretching, and its thickness is h_f.

Using (5.8) and (6.3), the cross-over velocity between both regimes is obtained

$$V_C = V^* \left(\frac{\alpha}{R_f}\right)^{3/4}. \tag{6.4}$$

For liquid mixtures in which $\alpha \sim 0.1$ nm and $R_f \sim 1$ mm, the cross-over velocity is of the order of 10^{-4}m s^{-1}, which is in the lowest range of accessible pulling velocities (Seiwert *et al.* 2014). As discussed in the Appendix A, for surfactant solutions, the length α with which they can be associated may be larger than the micron scale. In practice, however, it is difficult to provide an estimate for α, particularly at concentrations below the critical micellar concentration for which the dependence of surface tension on concentration is weak. A length $\alpha = 1$ µm corresponds to a critical velocity $V_C \approx 1$ m s^{-1}, a value that lies in the upper range of velocities reached in experiments. As a result, we expect the regime described by Frankel's laws to be generally met with surfactant solutions, except for very dilute solutions. In contrast, for liquid mixtures the experimental conditions always correspond to a regime with negligible drainage, in which an equilibrium of film tension is reached.

7. Conclusion

In summary, we have investigated the mechanisms responsible for the lifetimes of bubbles and foams in liquid mixtures, which are larger than those in pure liquids by four orders of magnitude. As a result of small concentration differences in the bulk and at the interfaces, the surface tension of liquid films is thickness dependent, which allows an equilibrium of film tension to be reached when a thin film forms. The equilibrium shape can be fully computed and the equilibrium thickness is predicted to vary with the square root of the length α that characterises the amplitude of the thickness dependence of surface tension. This prediction is in agreement with the experimental data obtained in single bubble and foaming experiments. In addition, we have found that, although the lifetimes of bubbles

are smaller by one order of magnitude than those of foams, their variations are remarkably identical, showing the same effects are at play. Finally, we discuss the differences between mixtures and surfactant solutions. In particular, we explain why formation of liquid films is controlled by the mechanism we invoke in mixtures, whereas it is generally controlled by drainage in surfactant solutions. We emphasise that liquid mixtures, and in particular oil mixtures, constitute well-controlled systems, in which the stabilising effect of foams and bubbles can be tuned by changing composition. In addition, their surface rheology is much simpler than that of surfactant solutions since it is purely elastic. For all these reasons, liquid mixtures provide model systems for quantitative studies aiming to better understand the mechanisms involved in the rupture of liquid films.

Acknowledgements. We warmly thank I. Cantat for enlightening discussions.

Declaration of interests. The authors report no conflict of interest.

Author ORCIDs.
L. Talini https://orcid.org/0000-0001-7309-7673.

Appendix A

We provide an estimate of the length α in the case of surfactant solutions. We assume for the sake of simplicity that surface and bulk concentrations are related through the Langmuir adsorption isotherm

$$\frac{c}{c_\infty} = \frac{\Gamma}{\Gamma_\infty - \Gamma}, \tag{A1}$$

where c is the surfactant bulk concentration and c_∞ that at the critical micellar concentration (c.m.c.), Γ is the number of moles per interface unit and Γ_∞ is that at the c.m.c.

We use the ideal approximation for surface tension

$$\gamma = \gamma_0 - RT\Gamma, \tag{A2}$$

together with surfactant conservation, in which we have introduced the thickness of the surfactant layer at the surface, $\delta = \Gamma_\infty v_M$, with v_M the molar volume of the surfactant

$$c_0 V = c(V - 2S\delta) + 2S\Gamma, \tag{A3}$$

and further using $h = 2V/S$, we finally obtain, in the limit of dilute solutions, i.e. for $c_\infty v_M \ll 1$

$$\Gamma(h) = \Gamma(h = \infty) - \frac{2}{h}\frac{c_0 c_\infty \Gamma_\infty^2}{(c_\infty - c_0)^3} + O\left(\frac{1}{h^2}\right). \tag{A4}$$

We emphasise that, in contrast to liquid mixtures, surfactant solutions are usually very dilute. With surfactants, the ratio of the surface and bulk concentrations is a length $\delta_s = \Gamma_\infty/c_\infty$, called the thickness of the subsurface and in the micrometre range. Introducing the reduced concentration $\hat{c} = c_0/c_\infty$, we obtain from (A1) and (A4)

$$\alpha \cong \delta_s \frac{RT\Gamma_\infty}{\gamma_0}\frac{2\hat{c}}{(1-\hat{c})^3}. \tag{A5}$$

Because $RT\Gamma_\infty/\gamma_0$ is in general of the order of unity, the value of α is in the micron range, but it can be smaller far below the c.m.c. and become considerably larger near the c.m.c.

References

Aradian, A., Raphael, E. & de Gennes, P.G. 2001 "Marginal pinching" in soap films. *Europhys. Lett.* **55**, 834–840.

Bikerman, J.J. 1973 *Measurement of Foaminess in Foams*. Springer.

Butler, J.A.V. 1932 The thermodynamics of the surfaces of solution. *Proc. R. Soc. Lond. Ser.* A-*Containing Papers Math. Phys. Character* **135**, 348–375.

Cantat, I., Cohen-Addad, S., Elias, F., Graner, F., Höhler, R., Pitois, O., Rouyer, F., Saint-Jalmes, A. & Cox, S. 2013 *Foams: Structure and Dynamics*. Oxford University Press.

Champougny, L., Roche, M., Drenckhan, W. & Rio, E. 2016 Life and death of not so "bare" bubbles. *Soft Matt.* **12**, 5276–5284.

Champougny, L., Scheid, B., Restagno, F., Vermant, J. & Rio, E. 2015 Surfactant-induced rigidity of interfaces: a unified approach to free and dip-coated films. *Soft Matt.* **11**, 2758–2770.

Chatzigiannakis, E. & Vermant, J. 2020 Breakup of thin liquid films: from stochastic to deterministic. *Phys. Rev. Lett.* **125**, 158001.

Culick, F.E.C. 1960 Comments on a ruptured soap film. *J. Appl. Phys.* **31**, 1128–1129.

Debregeas, G., de Gennes, P.G. & Brochard-Wyart, F. 1998 The life and death of "bare" viscous bubbles. *Science* **279**, 1704–1707.

Eberhart, J.G. 1966 The surface tension of binary liquid mixtures. *J. Phys. Chem.* **70**, 1183–1186.

Eriksson, J.C. 1964 On the thermodynamics of surface systems. *Adv. Chem. Phys.* **6**, 145–174.

Frostad, J.M., Tammaro, D., Santollani, L., de Araujo, S.B. & Fuller, G.G. 2016 Dynamic fluid-film interferometry as a predictor of bulk foam properties. *Soft Matt.* **12**, 9266–9279.

Gibbs, J.W. 1961 *Collected Works*, Vol. I, Dover Publishing.

Hosoi, A.E. & Bush, J.W.M. 2001 Evaporative instabilities in climbing films. *J. Fluid Mech.* **442**, 217–239.

Ivanov, I.B. 1988 *Thin Liquid Films: Fundamentals and Applications*. Marcel Dekker Inc.

Kendall, J. & Monroe, K.P. 1917 The viscosity of liquids. II. The viscosity-composition curve for ideal liquid mixtures. *J. Am. Chem. Soc.* **39**, 1787–1802.

Lhuissier, H. & Villermaux, E. 2012 Bursting bubble aerosols. *J. Fluid Mech.* **696**, 5–44.

Lorenceau, E. & Rouyer, F. 2020 Lifetime of a single bubble on the surface of a water and ethanol bath. *Phys. Rev. Fluids* **5**, 063603.

Mysels, K.J., Shinoda, K. & Frankel, S. 1959 *Soap Films: Studies of Their Thinning and a Bibliography*. Pergamon.

Prigogine, I. & Marechal, J. 1952 The influence of differences in molecular size on the surface tension of solutions .4. *J. Colloid Interface Sci.* **7**, 122–127.

Prins, A., Arcuri, C. & Vandente, M. 1967 Elasticity of thin liquid films. *J. Colloid Interface Sci.* **24**, 84–90.

Pugh, R.J. 1996 Foaming, foam films, antifoaming and defoaming. *Adv. Colloid Interface Sci.* **64**, 67–142.

Rio, E. & Biance, A.-L. 2014 Thermodynamic and mechanical timescales involved in foam film rupture and liquid foam coalescence. *Chemphyschem* **15**, 3692–3707.

Ross, S. & Nishioka, G. 1975 Foaminess of binary and ternary solutions. *J. Phys. Chem.* **79**, 1561–1565.

Santos, M.S.C.S. & Reis, J.C.R. 2014 New thermodynamics for evaluating the surface-phase enrichment in the lower surface tension component. *Chemphyschem* **15**, 2834–2843.

Scheid, B., Delacotte, J., Dollet, B., Rio, E., Restagno, F., van Nierop, E.A., Cantat, I., Langevin, D. & Stone, H.A. 2010 The role of surface rheology in liquid film formation. *Europhys. Lett.* **90**, 24002.

Seiwert, J., Dollet, B. & Cantat, I. 2014 Theoretical study of the generation of soap films: role of interfacial visco-elasticity. *J. Fluid Mech.* **739**, 124–142.

Shah, M.S., Kleijn, C.R., Kreutzer, M.T. & van Steijn, V. 2021 Influence of initial film radius and film thickness on the rupture of foam films. *Phys. Rev. Fluids* **6**, 013603.

Suja, V.C., Kar, A., Cates, W., Remmert, S.M., Savage, P.D. & Fuller, G.G. 2018 Evaporation-induced foam stabilization in lubricating oils. *Proc. Natl Acad. Sci. USA* **115**, 7919–7924.

van den Tempel, M., Lucassen, J. & Lucassen, E. 1965 Application of surface thermodynamics to gibbs elasticity. *J. Phys. Chem.* **69**, 1798–1804.

Tran, H.P., Arangalage, M., Jorgensen, L., Passade-Boupat, N., Lequeux, F. & Talini, L. 2020 Understanding frothing of liquid mixtures: a surfactantlike effect at the origin of enhanced liquid film lifetimes. *Phys. Rev. Lett.* **125**, 178002.

Tran, H.P., Delance, L., Passade-Boupat, N., Verneuil, E., Lequeux, F. & Talini, L. 2021 Foaming of binary mixtures: link with the nonlinear behavior of surface tension in asymmetric mixtures. *Langmuir* **37**, 13444–13451.